

# SPARSE MULTIVARIATE AUTOREGRESSIVE (MAR)-BASED PARTIAL DIRECTED COHERENCE (PDC) FOR ELECTROENCEPHALOGRAPH (EEG) ANALYSIS

Joyce Chiang, Z. Jane Wang

University of British Columbia  
Dept. of Electrical and Computer Engineering  
Vancouver, Canada

Martin J. McKeown

University of British Columbia  
Pacific Parkinson's Research Centre  
Vancouver, Canada

## ABSTRACT

Partial directed coherence (PDC) has recently been proposed for studying brain connectivity in EEG studies. PDC provides a quantitative spectral measure of the causal relations between signals by its central use of a multivariate autoregressive (mAR) model. Yet, in real applications, the successful estimation of PDC depends on the accuracy of mAR parameter estimation, which is often sensitive to the data size and model order. In addition, it is generally believed that connections between EEG nodes (brain regions) may be sparse. To address these concerns, we propose a sparse mAR-based PDC technique where PDC estimates are computed from sparse mAR coefficient matrices derived from penalized regression. The proposed technique is applied to both simulated data and real EEG recordings, and results show enhanced stability and accuracy of the proposed technique compared to the traditional, non-sparse approach. The sparse mAR-based PDC technique is promising for analyzing brain connectivity in EEG analysis.

**Index Terms**— Partial directed coherence (PDC), sparse multivariate autoregressive (mAR) model, EEG, penalized regression, brain connectivity.

## 1. INTRODUCTION

In neurobiology, there has been increasing interest in identifying functional connectivity between brain regions. Such connectivity is believed to provide an integrating framework for a variety of complex brain functions. Several mathematical methods have been explored in the literature to provide a quantitative measure of brain connectivity using electroencephalography (EEG) data, including correlation, coherence and Granger causality [1, 2]. Among them, spectral coherence, probably the most popular one, has been used extensively in EEG studies to investigate issues such as cortical synchrony during cognitive tasks and disrupted brain connectivity in pathological conditions. However, coherence technique has several limitations. First, it is a bivariate technique, meaning that only two signals are considered at a time. Yet, in most cognitive tasks, large number of brain regions are simultaneously interacting with each other. By doing pairwise analysis, coherence technique ignores possible critical influences by other brain regions and thus may lead to misleading results. Moreover, coherence is unable to identify the direction of information flow between cortical regions. Another recently proposed technique of neurobiological interest is Granger causality, as it provides a measure of causal relation between two

time series, but similar to coherence, Granger causality also only allows multiple pairwise analyses when considering the multichannel case [2].

To overcome these limitations, partial directed coherence (PDC) was later proposed for EEG connectivity studies, which extends the concepts of coherence and Granger causality to process multiple time series simultaneously. The PDC technique has the advantage of allowing the simultaneous modeling of all channels with a multivariate autoregressive (mAR) model, which gives a more accurate estimation of causality than a bivariate technique. PDC also allows the differentiation of direct and indirect causal influences among interacting entities. Moreover, since neural signals often exhibit frequency-specific oscillatory activity, the ability of providing spectral information of causal relations makes PDC an attractive tool for neuroscience studies. Examples of applications of PDC to real data include the study of brain networks in rats during different behavioral states [3] and the identification of oscillatory brain interactions in human during object recognition [4].

However, the computation of PDC in real applications poses technical challenges. As noted in [1], the successful estimation of PDC depends both on the proper fitting of the mAR model to the data and also the accuracy of the specific parameter estimations, which are dependent upon optimal mAR model order selection and adequate sample sizes of training data. In general, a higher model order allows more data dynamics to be captured and gives a higher frequency resolution, but at the expense of a greater number of parameters to be estimated. More parameter estimations may create statistical instability for ordinary maximum likelihood estimators when only limited observations are available [5]. Thus, it is of critical importance in practice to make a good trade-off between model complexity and estimation accuracy. In addition, the underlying implicit full connection assumption in a regular mAR model used for PDC is questionable in EEG connectivity analysis, especially when the effects of volume conduction, which may erroneously suggest connections between channels, are account for. In other words, the connections between EEG nodes (or brain regions) may be considered *a priori* to form a sparse network.

The above observations motivate us to incorporate a sparse mAR model into the current PDC technique. In an effort to resolve a similar concern in functional Magnetic Resonance Imaging (fMRI) studies, Valdés-Sosa *et al.* [5] proposed modeling fMRI data using sparse mAR models in which the parameters are estimated using penalized regression. By using penalized regression, many regression coefficients are shrunk to zero during the estimation process. The resulting mAR coefficient matrix will thus have sparse structures, meaning that only small number of elements are non-zero. In this paper, we propose the sparse mAR-based PDC technique in which PDC esti-

This study was supported by Canadian federal funding agencies NSERC (under STPGP 365208-08) and CIHR.

mates are computed using sparse mAR coefficient matrices given by penalized regression. Penalized regression effectively reduces the number of free parameters to be estimated, which is particularly important when the data is of limited sample size. We evaluate the performance of the proposed approach using both simulated data and real EEG data.

This paper is organized as follows: in Section 2, we will describe the regular and sparse mAR models and the parameter estimation techniques. The PDC estimate is defined in Section 2.2. In Section 3, the performance of regular mAR- and sparse mAR-based PDC will be compared. Finally, we conclude in Section 4.

## 2. METHODS

We first review regular multivariate autoregressive models and least square-based parameter estimation techniques. We then introduce the concept of sparse mAR and present penalized regression methods for solving such sparse problems. Finally, the definition of partial directed coherence is given in Section 2.2.

### 2.1. Sparse mAR Model

In a regular mAR model, the multivariate time series at each time point is represented as a linear, weighted sum of its previous time points, and it can be formulated as

$$\mathbf{y}(t) = \sum_{r=1}^p \mathbf{A}_r \mathbf{y}(t-r) + \mathbf{e}(t), \quad (1)$$

where the observation  $\mathbf{y}(t)$  is a  $d$ -dimensional vector at time  $t$ ,  $p$  denotes the order of mAR model, and the vector  $\mathbf{e}(t)$  represents white Gaussian noise. The mAR coefficient  $\mathbf{A}_r$  is a  $d \times d$  matrix, where the element  $A_r(i, j)$  measures the influence that variable  $j$  exerts on variable  $i$  after  $r$  time points. In the regression framework, Eqn. 1 can be rewritten as

$$\mathbf{Z} = \mathbf{X}\boldsymbol{\beta} + \mathbf{E} \quad (2)$$

where

$$\begin{aligned} \mathbf{Z} &= \mathbf{Y}_{p+1:N} \\ &= [\mathbf{y}(p+1), \mathbf{y}(p+2), \dots, \mathbf{y}(N)]^T, \\ \mathbf{X} &= [\mathbf{Y}_{p:N-1}, \mathbf{Y}_{p-1:N-2}, \dots, \mathbf{Y}_{1:N-p}], \\ \boldsymbol{\beta} &= [\mathbf{A}_1, \mathbf{A}_2, \dots, \mathbf{A}_p]^T, \\ \mathbf{E} &= [\mathbf{e}(p+1), \mathbf{e}(p+2), \dots, \mathbf{e}(N)]^T. \end{aligned}$$

Eqn. 2 can be solved using the maximum likelihood (ML) approach. Under the iid white noise assumption of  $\mathbf{E}$ , this is equivalent to minimizing the mean square error:

$$\hat{\boldsymbol{\beta}} = \arg \min_{\boldsymbol{\beta}} \|(\mathbf{Z} - \mathbf{X}\boldsymbol{\beta})\|^2. \quad (3)$$

It is worth emphasizing that the performance of the ML estimator is highly dependent on the sample size  $N$  and the number of parameters to be estimated. In real world applications, the available data points are often limited, which in turn leads to poor estimation accuracy. Furthermore, the estimated coefficients yielded by the least square (LS) approach in Eqn. 3 are typically non-zero, which makes neurobiological interpretation of results difficult (e.g. identifying brain connectivity patterns in EEG studies). Such non-zero observation is also against the sparsity assumption in brain connectivity networks.

To address these issues, a possible solution is to impose sparsity constraint on the mAR coefficients (i.e.  $\mathbf{A}_r$  matrix) and perform variable selection using penalized regression methods [5]. The basic idea of penalized regression is to maximize the likelihood while at the same time, penalize complex models. In terms of mathematical formulation, penalized regression can be expressed as the minimization of the penalized least square function:

$$\hat{\boldsymbol{\beta}} = \arg \min_{\boldsymbol{\beta}} \|(\mathbf{Z} - \mathbf{X}\boldsymbol{\beta})\|^2 + \lambda^2 \sum_{j=1}^d p(|\beta_j|), \quad (4)$$

where  $\lambda$  is the regularization parameter which controls the amount of penalization imposed on the solution and it can be determined using Bayesian information criterion (BIC).  $p(|\beta_j|)$  is the penalty function applied to each regression coefficient. Several different penalty functions have been introduced, including ridge, LASSO and SCAD. An overview of these penalty functions can be found in [6]. In this paper, LASSO penalization,  $p(|\beta_j|) = |\beta_j|$ , is chosen because of its ability to automatically set small estimated coefficients to zero, which naturally result in sparse solution. This special property, also known as the *sparsity property*, is particularly useful in variable selection problems.

To solve the optimization problem in Eqn. 4, the technique we use is the Local Quadratic Approximation (LQA) algorithm, proposed by Fan and Li [6]. LQA first casts the problem of penalized least square minimization presented in Eqn. 4 into a penalized likelihood maximization problem. It further addresses the issue of *singularity at the origin* that exists in penalty functions such as LASSO and SCAD by locally approximating  $p(|\beta_j|)$  with a quadratic function. The resulting penalized likelihood function becomes both differentiable and concave, and it can easily be solved using Newton-Raphson optimization algorithm. A detailed description of the LQA algorithm can be found in [6].

### 2.2. Partial Directed Coherence

PDC can be considered as the frequency-domain representation of Granger causality. It involves the transformation of the mAR coefficients in Eqn. 2 into the frequency domain via the Fourier transform

$$\bar{\mathbf{A}}(f) = \mathbf{I} - \sum_{r=1}^p \mathbf{A}_r e^{-i2\pi f r}, \quad (5)$$

where  $\mathbf{I}$  is a  $d \times d$  identity matrix. The estimate of PDC from the node  $y_i$  to the node  $y_j$  is defined as

$$\pi_{y_j \leftarrow y_i}(f) = \frac{\bar{A}_{j,i}(f)}{\sqrt{\sum_{m=1}^d |\bar{A}_{m,i}(f)|^2}}. \quad (6)$$

PDC takes on a value between 0 and 1. It essentially measures the relative interaction strengths with respect to a given source signal. The PDC  $\pi_{y_j \leftarrow y_i}(f)$  describes the linear pairwise relatedness between  $y_i$  and  $y_j$  as a function of frequency after discounting the effect of other simultaneously observed series.

## 3. RESULTS

In this section, we will first examine the PDC results produced by sparse mAR models and by regular mAR models when fitted to simulated data. Next, we will present a case study where the proposed sparse mAR-based PDC is applied to real EEG data collected from an motor task where visual stimuli were presented in a virtual environment.

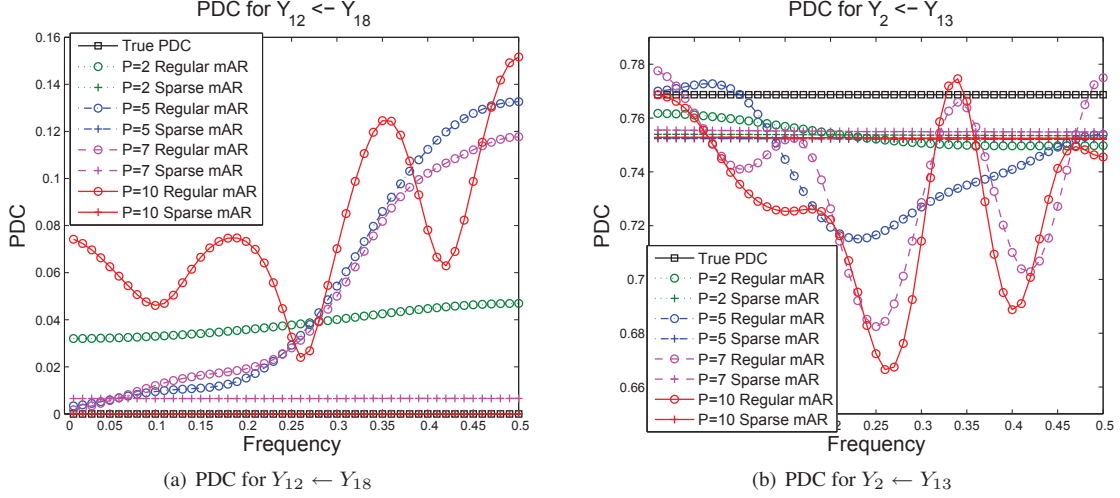


Fig. 1. PDC from Simulated Data

### 3.1. Simulated Data

To compare the PDC estimates produced by sparse mAR models and by regular mAR models, a 18-channel, second-order (i.e.  $p = 2$ ) mAR system is simulated. The noise term  $\mathbf{e}(t)$  is white Gaussian noise with zero-mean and unit variance, and the data length is set to 3,000 points. Note that such a short data length is purposely chosen as to illustrate the effects of estimation errors in mAR coefficients on PDC values. The mAR coefficient matrices are  $18 \times 18$  sparse matrices whose non-zero elements are given by

$$\begin{aligned}
 A_1(2, 13) &= 0.95\sqrt{2}, & A_2(1, 1) &= -0.9025, \\
 A_1(2, 1) &= -0.5, & A_2(3, 2) &= 0.4, \\
 A_1(10, 13) &= -0.5, & A_2(16, 18) &= -0.2, \\
 A_1(13, 14) &= 0.25\sqrt{2}, & A_2(4, 16) &= 0.7, \\
 A_1(10, 2) &= 0.25\sqrt{2}, \\
 A_1(5, 4) &= -0.25\sqrt{2}, \\
 A_1(5, 5) &= 0.25\sqrt{2}.
 \end{aligned}$$

To investigate the effects of model order estimates (i.e. choice of  $p$  in Eqn. 2) on PDC, regular and sparse mAR models of order 2, 5, 7 and 10 are fitted to the simulated data. The resulting PDC curves of selected connections are plotted in Fig. 1. We first demonstrate an example by looking at the PDC from channel 18 to channel 12 as shown in Fig. 1(a). Given that  $A_1(12, 18) = A_2(12, 18) = 0$ , the true PDC is  $\pi_{12 \leftarrow 18}(f) = 0$ , indicating the absence of direct causal influence from channel 18 to channel 12. When the PDC is calculated based on  $\mathbf{A}_p$  given by the sparse mAR models, regardless of the choice of model order, the estimated PDC curves (lines with crosses as markers) are exactly the same as the true PDC (line with squares) at all frequencies, except when  $p = 10$ , the estimated PDC is slightly greater than zero ( $\pi_{12 \leftarrow 18}(f) \sim 0.007$ ). On the other hand, the estimated PDC given by regular mAR (lines with circles) noticeably deviates from the true PDC and the deviation increases as the model order increases. When statistical tests are applied, the estimated PDC given by regular mAR is highly likely to be considered statistically significant, even though there is no causal influence from  $Y_{18}$  to  $Y_{12}$  in the true model. Similar observations are also noted in other connections. This ultimately results in falsely identified connectivity patterns.

One non-zero connectivity example we look at is from channel 13 to channel 2. In this case, as shown in Fig. 1(b), the true PDC

$\pi_{2 \leftarrow 13}$  takes on the value of 0.769 at all frequencies. The sparse mAR-based PDC estimates provide very close approximation to the true values and the deviations are around 0.01 for all model orders. In the case of regular mAR, similar to the connection from  $Y_{18}$  to  $Y_{12}$ , the PDC estimates differ from the true PDC considerably. One observation worth pointing out is that, when  $p = 10$ , the traditional PDC estimate fluctuates substantially across considered frequencies. This artifact arises from the estimation errors incurred when highly complex mAR models are trained by limited data points, and it may lead to misleading interpretations of spectral properties of the underlying system.

### 3.2. Case Study: EEG Analysis

Next, we apply the proposed technique to the EEG data collected from a virtual reality experiment. In this experiment, 7 healthy subjects were recruited and asked to respond to visual stimuli in a computer-simulated virtual environment. The stimuli consists of 150 virtual balls that were sequentially launched and loomed directly towards the subject. Among these 150 balls, 50% of the balls were distracter balls and the other 50% are target balls. The distracter balls remained white in color during the course of their trajectory whereas the target balls were initially launched as distracter balls (i.e. white in color) and after approximately 1.5 seconds, the target balls revealed itself by changing color from white to blue. Subjects were instructed to ignore distracter balls and reach out to block target balls with a virtual paddle as soon as they turned blue.

To record the brain activity, subjects were fitted with an EEG cap with 18 active channels placed according to the international 10-20 placement systems. The placement of the electrodes is shown in Fig. 2, and they are, starting from the top left corner, FP1, FP2, F7, F3, FZ, F4, F8, T7, C3, CZ, C4, T8, P7, P3, PZ, P4, O1 and O2. Two additional electrodes were placed above and below the eye for detecting eye-movement artifacts. EEG signals were recorded using the SynAmps<sup>2</sup> amplifier and Scan4 software (NeuroScan<sup>®</sup>, Compumedics<sup>®</sup>, Texas, USA). The data were digitally sampled at 1000Hz and later downsampled to 250Hz. To eliminate eye artifacts, Independent Component Analysis (ICA) was applied to the EEG recordings using the procedure described by Jung *et al.* in [7]. The denoised data were bandpassed between 5-100Hz.

For the analysis, only EEG signals collected during the course

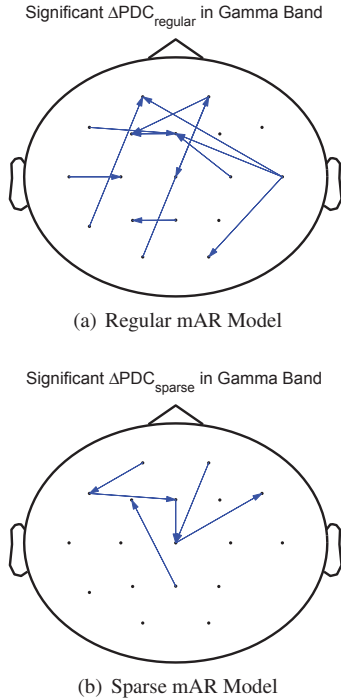


**Fig. 2.** Head plots showing significant connections in Gamma band (36-60Hz). (a) Significant connections as determined by t-test on  $\Delta PDC_{regular}$  (b) Significant connections as determined by t-test on  $\Delta PDC_{sparse}$

of successfully blocked target balls are used. Moreover, for each target ball, the EEG signals are segmented into two parts: *pre-reveal* period, which is between the time the target was launched and the time the target revealed itself, and *post-reveal* period, which is between the time the target revealed itself and the time the target was blocked by the subject. Third order regular mAR models and third order sparse mAR models are separately fitted to the *pre-reveal* period and *post-reveal* period. PDC values are calculated based on the estimated mAR coefficients. To study the effects of ball launch, PDC values from *pre-reveal* period is subtracted from *post-reveal* period. Let  $\Delta PDC_{regular}$  and  $\Delta PDC_{sparse}$  denote the PDC differences given by regular mAR and sparse mAR, respectively. Student t-tests are separately applied to  $\Delta PDC_{regular}$  and  $\Delta PDC_{sparse}$ , and the significant connections are shown in Fig. 2. The  $\Delta PDC_{sparse}$  results are consistent with demonstrating frontal gamma synchronization in the frontal area of cortex in response to complex visual stimuli requiring interpretation [8]. In particular, the  $\Delta PDC_{regular}$  and  $\Delta PDC_{sparse}$  curves for the connection from F7 to FZ, which is shared by both regular mAR and sparse mAR models, is shown in Fig. 3. The midline of the  $\Delta PDC_{sparse}$  curves are more consistent across subjects, as shown by the standard deviation in Fig. 3.

#### 4. CONCLUSION

The proposed sparse MAR-based PDC estimates are shown to be more accurate and consistent in simulations. In a real EEG study, the results from the sparse MAR-based PDC approach were consistent with prior studies emphasizing frontal gamma oscillations. Our results suggest that when the number of data points are limited as often the case in real word applications, the sparse MAR-based PDC

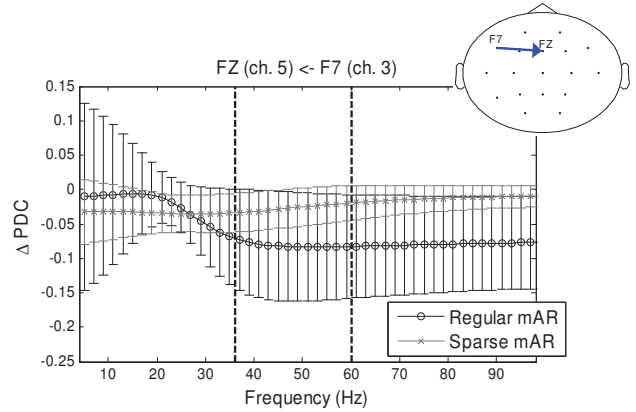


**Fig. 3.**  $\Delta PDC_{regular}$  and  $\Delta PDC_{sparse}$  curves for the connection from F7 to Fz. The vertical lines represent the standard deviation. The two vertical dashed lines delimit the Gamma frequency band which ranges from 36 to 60Hz.

formulation is more suitable for real EEG analysis by accommodating the sparse nature of brain connectivity network and naturally addressing the concern of model order selection, and that PDC results based on the regular MAR approach should be interpreted with caution.

#### 5. REFERENCES

- [1] E. Pereda, R. Quiroga, and J. Bhattacharya, "Nonlinear multivariate analysis of neurophysiological signals," *Progress in Neurobiology*, vol. 77, no. 1-2, pp. 1-37, 2005.
- [2] L. Baccalá and K. Sameshima, "Partial directed coherence: a new concept in neural structure determination," *Biological Cybernetics*, vol. 84, no. 6, pp. 463-474, 2001.
- [3] E. Fanselow, K. Sameshima, L. Baccala, and M. Nicolelis, "Thalamic bursting in rats during different awake behavioral states," *Proceedings of the National Academy of Sciences*, vol. 98, no. 26, p. 15330, 2001.
- [4] G. Supp, A. Schlögl, N. Trujillo-Barreto, M. Müller, and T. Gruber, "Directed Cortical Information Flow during Human Object Recognition: Analyzing Induced EEG Gamma-Band Responses in Brain's Source Space," *PLoS ONE*, vol. 2, no. 8, 2007.
- [5] P. Valdés-Sosa, J. Sánchez-Bornot, A. Lage-Castellanos, M. Vega-Hernández, J. Bosch-Bayard *et al.*, "Estimating brain functional connectivity with sparse multivariate autoregression," *Philosophical Transactions of the Royal Society B: Biological Sciences*, vol. 360, no. 1457, pp. 969-981, 2005.
- [6] J. Fan and R. Li, "Variable Selection via Nonconcave Penalized Likelihood and its Oracle Properties," *Journal of the American Statistical Association*, vol. 96, no. 456, pp. 1348-1360, 2001.
- [7] T. Jung, C. Humphries, T. Lee, S. Makeig, M. McKeown *et al.*, "Extended ICA removes artifacts from electroencephalographic recordings," *Advances in Neural Information Processing Systems*, vol. 10, pp. 894-900, 1998.
- [8] C. Başar-Eroglu, D. Strüber, P. Kruse, E. Başar, and M. Stadler, "Frontal gamma-band enhancement during multistable visual perception," *International Journal of Psychophysiology*, vol. 24, no. 1-2, pp. 113-125, 1996.